Ollscoil na Gaillimhe
University of Galway

Provided by the author(s) and University of Galway in accordance with publisher policies. Please cite the published version when available.

Title	A kinetic modelling study of alcohols operating regimes in a HCCI engine
Author(s)	Pelucchi, Matteo; Bissoli, Mattia; Rizzo, Cristina; Zhang, Yingjia; Somers, Kieran; Frassoldati, Alessio; Curran, Henry J.; Faravelli, Tiziano
Publication Date	2017-09-04
Publication Information	Pelucchi, Matteo, Bissoli, Mattia, Rizzo, Cristina, Zhang, Yingjia, Somers, Kieran, Frassoldati, Alessio, Curran, Henry J., Faravelli, Tiziano. (2017). A Kinetic Modelling Study of Alcohols Operating Regimes in a HCCI Engine. SAE Int. J. Engines, 10(5), 2354-2370. doi: 10.4271/2017-24-0077
Publisher	SAE International
Link to publisher's version	https://doi.org/10.4271/2017-24-0077
Item record	http://hdl.handle.net/10379/14809
DOI	http://dx.doi.org/10.4271/2017-24-0077

Downloaded 2024-04-26T04:07:07Z

Some rights reserved. For more information, please see the item record link above.

20XX-01-XXXX

A Kinetic Modelling Study of Alcohols Operating Regimes in a HCCI Engine

Author, co-author (Do NOT enter this information. It will be pulled from participant tab in MyTechZone)
Affiliation (Do NOT enter this information. It will be pulled from participant tab in MyTechZone)

Abstract

Pursuing a sustainable energy scenario for transportation requires the blending of renewable oxygenated fuels such as alcohols into commercial hydrocarbon fuels. From a chemical kinetic perspective, this requires the accurate description of both hydrocarbon reference fuels (*n*-heptane, *iso*-octane, toluene, etc.) and oxygenated fuels chemistry. A recent systematic investigation of linear C_2–C_5 alcohols ignition in a rapid compression machine at p = 10–30 bar and T = 650–900 K has extended the scarcity of fundamental data at such conditions, allowing for a revision of the low temperature chemistry for alcohol fuels in the POLIMI mechanism. Heavier alcohols such as *n*-butanol and *n*-pentanol present ignition characteristic of interest for application in HCCI engines, due to the presence of the hydroxyl moiety reducing their low temperature reactivity compared to the parent linear alkanes (i.e. higher octane number). The promising performances of ethanol in a HCCI engine have been recently discussed by Bissoli et al. (*Energy & Fuels, 2017, Submitted*), observing wider stable operability conditions in terms of fuel/air load (λ) and exhaust gas recirculation (EGR) extent compared to PRF80 and PRF100. The aim of this study is to present briefly the reliability of the updated POLIMI mechanism for heavier alcohols and to investigate the fundamental role of chemical kinetics on the performance maps of HCCI engines fueled with *n*-butanol and *n*-pentanol, in terms of operability limits and engine efficiency.

1. Introduction

Modern society is facing multifaceted and complex energy-related challenges. Projection for the next 20-30 years foresee the combustion of fossil fuels to keep driving energy production, mostly due to higher energy demands for road, air and sea transport [1]. While suitable alternatives to combustion exist for power generation, transportation requires high energy density sources, i.e. petroleum-derived liquid fuels (gasoline, diesel, kerosene, naphta). Moreover, environmental issues associated to combustion, pollution reduction targets [2] and other political and economic strategies endorse the use of biofuels (neat or in blends with commercial fuels) as the most promising near term alternative to fossil fuels for internal combustion engines.

First-generation fatty acid methyl-esters [3, 4] together with second-generation biofuels such as alcohols [5] and furans [6] have been one of the main topic of combustion chemistry research in the last decade. Particularly, large interest has been devoted to alcohols, due to the viable production pathways from biological matter [7, 8].

Starting from bioethanol, nowadays blended with gasoline up to 85% (E85 gasoline) and used in fuel flexible vehicles, an increasing interest in higher alcohols, with four or more carbon atoms has emerged because of favorable physical and thermodynamic properties [5]. Energy density, heating value, viscosity, hygroscopicity and volatility of higher alcohols are in fact compatible with the requirements of existing distribution infrastructure (pipe lines, tanks etc.) and most importantly with modern engines. Therefore, the interest in C_4-C_6 alcohols as fuel additives or as replacements for fossil fuels.

In the United States, the Octamix waiver [9] already allowed up to 16% butanol blends with gasoline as an equivalent to E10 gasoline. Many studies investigated the performances of biobutanol as a fuel or fuel additive. Rakopoulos et al. [10] as well as Siwale et al. [11] investigated blends of up to 24% v/v butanol in diesel, observing generally improved exhaust emission quality. Also a decrease in soot emissions was highlighted by Valentino et al. [12], due to the lower ignitability of butanol/diesel blends.

Pentanol is also an attractive second-generation bio-fuels and can be produced from renewable feedstock. Its higher energy density, higher heating value, higher viscosity, lower hygroscopicity and lower volatility [5] motivated the interest in pentanol isomers. Campos-Fernandez et al. [13] investigated power and fuel economy performance of diesel/pentanol blends (10-25% v/v of pentanol) in a direct injection compression ignition engine. Wei et al. [14] tested blends with up to 30% pentanol by volume. Li et al. experimentally investigated the emission performance, fuel economy and combustion characteristic of neat pentanol in a diesel engine [15]. Overall these studies highlighted the potentials of the use of n-pentanol in diesel engines. Table 1 shows some important properties of several alcohols, gasoline and diesel fuels such as the lower heating value (LHV), research octane number (RON), motor octane number (MON) and cetane number (CN).

Table 1: Properties of alcohols, gasolines and diesel fuels. Adapted from Sarathy et al. [5] and Kalghatgi [16].

Fuel	LHV (MJ/L)	RON	MON	CN
Gasoline	~30-33	88-98	80-88	n.d.
Diesel	~35	n.d.	n.d.	40-55
n-butanol	26.9	98	85	12
n-pentanol	28.5	80	74	20
n-hexanol	29.3	56	46	24

Correctly assessing the reactivity of a new fuel or a new gasoline or diesel formulation is largely a chemical kinetics problem. A better understanding of a specific chemical compound's effects on combustion performances (flame speed, auto-ignition etc.) and emission allow the design of a fuel or fuel blend for an existing technology, the tuning of an engine for an assigned fuel or the concerted development of fuels and engines [17]. Typical surrogate mixtures such as primary reference fuels (PRFs) and toluene reference fuels (TRFs) have started to include different alcohols to investigate their possible impact on commercial fuels [18]. From a chemical kinetic perspective, an accurate description of the combustion chemistry of every surrogate component (n-heptane, iso-octane, toluene, ethanol, butanol etc.) is imperative. The recent review of Sarathy et al. [5] discussed the state of the art understanding of alcohols combustion chemistry, synoptically pointing out many improvement margins and open questions. Following the inputs of Sarathy et al. [5], a joint research effort between the CRECK group at Politecnico di Milano (POLIMI) and the C3 group at National University of Ireland, Galway (NUIG) investigated the auto-ignition propensity of *n*-C_2-C_5 alcohols in a twin-piston Rapid Compression Machine (RCM), with the aim of systematically revising alcohols low temperature chemistry.

Along with new fuel formulations to be used in conventional spark ignition (SI) and compression ignition (CI) engines, new engine technologies are also being investigated [16]. Homogeneous Charge Compression Ignition (HCCI) engines have received great attention in the last few decades because of the possibility to obtain high power

output with a cleaner combustion [19]. In HCCI engines, fuel and air are fully premixed, as in conventional SI engines, and the charge is ignited through compression, relying on its auto-ignition characteristics, like in CI engines. Although the use of a premixed air-fuel charge ensures reduced NOx and soot emissions, it also causes High Heat Release (HRR) and Pressure Rise Rates (PRR) leading to ringing events [20], strongly limiting the power output. Charge dilution by means of lean equivalence ratio and Exhaust Gas Recirculation (EGR) allow preventing these phenomena, but excessive charge dilution leads to very low power output and unburned hydrocarbon emissions. Typical undesired phenomena such as knock, already limiting the efficiency of SI engine, are also an issue in HCCI engines, with the additional criticism derived from the lack of cycle control measures such as spark timing (SI engine) or fuel injection timing (CI engine).

Beside extensive experimental investigations of HCCI operating ranges, also including neat *n*-butanol or blends in the most recent literature [21-25], some computational model providing a time- and cost-effective solution to analyze and optimize the engines, have been reported in the literature [26-32]. In particular, stemming from the well-recognized fundamental role of chemical kinetics in HCCI combustion, and from the general lack of knowledge about the chemical phenomena ruling HCCI operability maps, Bissoli et al. (*Energy & Fuels, 2017, Submitted*) validated a multi-zone model to study the impact of different fuels and engine configurations (speed and boost) on the operability maps, from a chemical point of view, by means of advanced tools like Sensitivity Analysis and Rate of Production Analysis [32].

Starting from the description and validation of the updated POLIMI alcohols mechanism, this study investigates the chemical kinetics underlying the operability maps and efficiency of HCCI engines fueled with *n*-butanol, *n*-pentanol and a TRF/butanol gasoline surrogate [33].

The manuscript is organized as follows. Section 2 briefly discusses the experimental approach at NUIG also comparing alcohols ignition-delay time measurements with previous measurements from the literature. The kinetic mechanism of *n*-butanol and *n*-pentanol is then discussed, mostly focusing on the low temperature oxidation pathways. Comparison of experimental data with POLIMI model predictions for *n*-butanol, *n*-pentanol and PRF-TRFs/butanol mixtures is presented to prove reliability of the chemistry. Section 3 describes the main features of the multi-zone HCCI model and its validation method. Section 4 discusses operability and performance maps of HCCI engines charged with the same fuels for which ignition propensity is discussed in Section 2.

2. Kinetic Model of *n*-butanol and *n*-pentanol Low Temperature Combustion

Modelling the autoignition in HCCI engines requires an accurate description of low and high temperature combustion kinetics of alcohols. Moving from the studies on propanol isomers by Frassoldati et al. [34] and of butanol isomers by Grana et al. [35], the high temperature kinetic mechanism has been recently revised and extended to pentanol isomers (*n*- and *iso*-pentanol) [36]. A lumped low temperature mechanism to describe *n*-butanol oxidation was proposed by Pelucchi et al. [37]. Starting from a systematic evaluation of the influence of different oxygenated functional groups on C-C and C-H bonds strength, a description of the main features and reaction pathways characterizing the reactivity of different oxygenated fuels (alcohols, aldehydes, ketones, methyl esters) was provided, with particular focus on intermediate and low temperature regimes [37]. The same rules applied to *n*-butanol, were then extended to describe *n*-pentanol oxidation at low temperatures, according to the assumption that the effect of the functional group vanishes after the β position [37-39], as schematically represented in Figure 1.

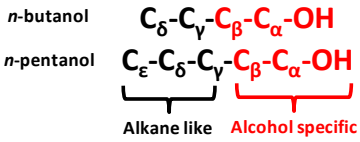

Figure 1: treatment of different carbon positions in *n*-butanol and *n*-pentanol.

Stemming from the lack of a systematic investigation of alcohols auto-ignition chemistry under engine relevant conditions and from the scarcity of measurements at low temperatures and high pressures [5], ignition delay times were measured in the twin-piston rapid compression machine (RCM) at NUIG for *n*-butanol and *n*-pentanol/"air" stoichiometric mixtures at p=10-30 bar and T=700-925 K. The extended experimental targets for model validation guided a revision of the lumped low temperature mechanism, as discussed in Section 2.2.

New fuels formulation requires the coupling of alcohols chemistry with standard PRFs and TRFs surrogates, representative of commercial fuels [33, 40]. The global POLIMI mechanism has been thoroughly validated for pure component such as *n*-heptane, *iso*-octane and toluene and their mixtures [41-43]. The mechanism uses a lumped description of the primary propagation reactions of larger species and primary intermediates [44, 45]. This approach, together with an extensive use of structural analogies and similarities within the different reaction classes, easily allows extension of the scheme to new species (e.g. *n*-hexanol), still maintaining a relatively low number of species (298 species, 11095 reactions). The kinetic mechanism, together with thermodynamic properties is provided in the Supporting Information.

2.1 Experimental Methodology

Ignition delay time measurements were carried out in the rapid compression machine described by Darcy et al. [46] at NUIG. *n*-butanol (≥99%) and n-pentanol (≥99%) were obtained from Sigma–Aldrich, while helium (99.9%), oxygen (99.5%), argon (99.9995%), nitrogen (99.95%), and carbon dioxide (99.5%) were supplied by BOC Ireland. Auto-ignition measurements for *n*-butanol and *n*-pentanol/"air" stoichiometric mixtures were conducted at temperatures of ~700-925 K, and pressures of 10–30 bar. Mixture compositions are reported in Table 2.

Table 2: Φ=1.0 alcohols / "air" mixture compositions (% mole fraction) tested in this study.

n-butanol					
Mixture	Fuel	O2	N2	Ar	CO2
Mix1-C4, p=30 bar	3.38	20.29	68.70	7.63	0.00
Mix2-C4, p=10 bar	3.38	20.28	15.26	61.09	0.00
Mix3-C4, p=30 bar	3.39	20.36	53.61	0.00	22.63

n-pentanol					
Mixture	Fuel	O2	N2	Ar	CO2
Mix1-C5, p=10 bar	2.72	20.43	76.85	0.00	0.00
Mix2-C5, p=10 bar	2.72	20.43	38.42	38.42	0.00

The experimental data thus obtained agree well with previous literature measurements in RCM and Shock Tubes (ST). Deviations between measurements at similar conditions have to be attributed to differences in the facility design and in diluent compositions (N_2/Ar/CO_2) in data from different authors. Deviations from ideal behavior caused by heat loss and complex fluid dynamics were taken into account for RCM simulations. Volume histories necessary for the correct simulation of the new data presented in this study are reported in the Supporting Information.

*Figure 2*a shows simulated pressure profiles for n-butanol and *n*-pentanol at T_c=830 K and 838 K, respectively. Experimental ignition delay times of the two alcohols at p=10 bar are compared in *Figure 2*b, highlighting the higher low temperature reactivity of *n*-pentanol, and a converging ignition propensity for T>~950 K.

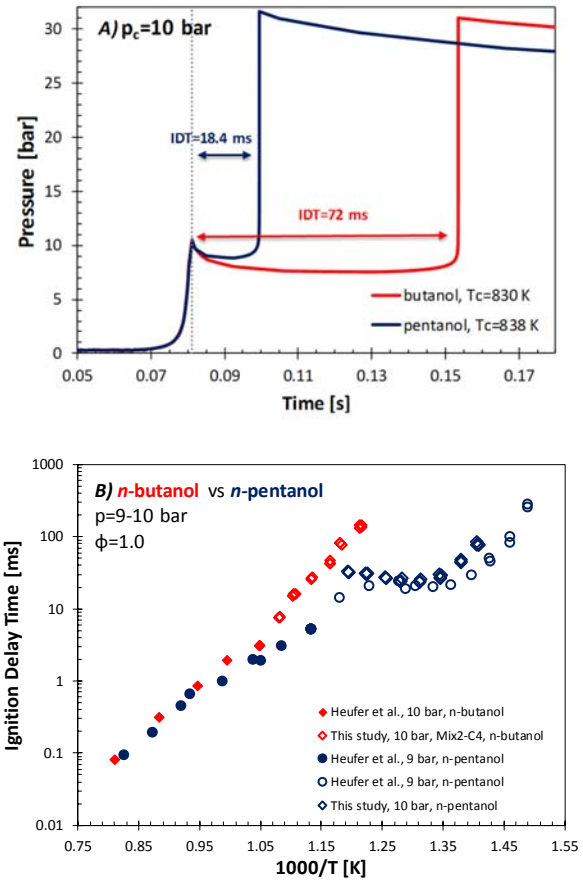

Figure 2: A) Calculated pressure history for *n*-butanol and *n*-pentanol stoichiometric mixtures at T_c~830-840 K and p_c~10 bar. B) Comparison between *n*-butanol and *n*-pentanol ignition delay measurements at P_c~10 bar. Open symbols: RCM experiments (this study □ and Heufer et al. ◊ [38]), full symbols: shock tube experiments [38].

2.2 Kinetic Mechanism

Prior to the systematic revision of *n*-butanol and *n*-pentanol kinetics, the thermodynamic properties of the fuels, fuel radicals (alkyl, peroxy, hydroperoxy alkyl etc.) and stable species (enols, ketohydroperoxides etc.) have been obtained based on the revised group contributions by Burke et al. [47]. Properties of the lumped low temperature species have been obtained as a selectivity based average of the different possible isomers. It has to be noted that, according to the lumping procedure proposed by Ranzi et al. [44, 45] both the forward and the reverse rate constant in the low temperature pathways are explicitly assigned, nullifying the effect of updated thermochemistry of typical low temperature species. Figure 3 shows bond dissociation energies (BDE) for *n*-butanol C-H and C-C bonds, highlighting the weakening effect of the hydroxyl functional group on vicinal bonds. As summarized in Figure 1 such effect vanishes after the β-positions.

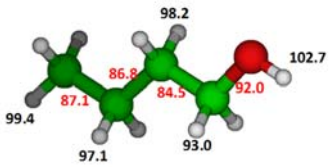

Figure 3: C−H (black) and C−C (red) bond dissociation energies (kcal mol^{-1}). Adapted from [37].

Fuel consumption mostly occurs through H-abstraction to form fuel radicals. OH and HO_2 are the dominant abstracting radical over the whole temperature range of interest for HCCI combustion. The observed bond strength hierarchy directly impacts relative selectivity to the different H-abstraction channels. Rate constants for H-abstraction by OH, HO_2 and CH_3 on alcohols-specific positions have been adopted from Zhou et al. [48-50]. Alkane-like positions are treated according to the systematic approach of Ranzi et al. [51], as already reported in previous studies [34-36].

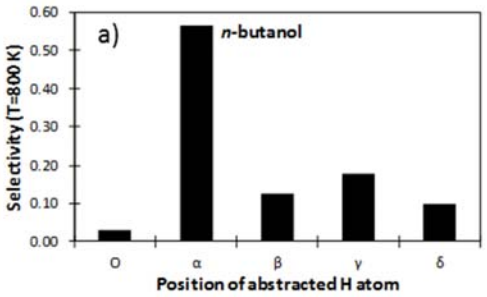

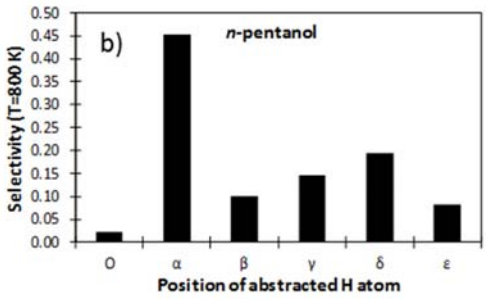

Figure 4: H-abstraction selectivity as a function of temperature from Rate of Production Analysis at T=800 K and p=30 bar.

Figure 4 shows selectivity of H-abstractions by OH for both *n*-butanol and *n*-pentanol. As expected from the BDEs, the formation of α radical largely dominates, followed by the secondary alkane-like positions (γ in *n*-butanol or γ and δ in *n*-pentanol), and by the secondary β position, whose C-H bond is ~1 kcal mol^{-1} stronger than the alkane-like secondary positions. H-abstraction from the hydroxyl group only accounts for ~5 % of the overall selectivity.

Similarly to alkanes, the fuel radical can isomerize or decompose via β-scission reactions [52]. At lower temperatures alkyl radicals interact with oxygen forming peroxy radicals, activating the typical low temperature reaction pathways [5, 44, 53]. A schematic representation of the low temperature oxidation mechanism of alcohols is given in Figure 5, highlighting pathways that are particularly relevant or new pathways with respect to alkanes (thicker arrows).

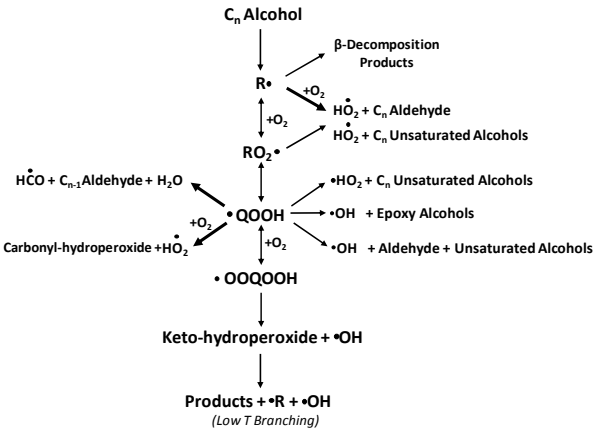

Figure 5: Schematic representation of alcohols low temperature oxidation mechanism. Thicker arrows represent new or particularly relevant pathways in alcohols oxidation with respect to alkanes.

The peculiarity of alcohols oxidation at low temperatures is that the α-hydroxyalkylradical (R-·CH-OH) reacts with O_2 to rapidly form HO_2 and the parent aldehyde or ketone without forming stable peroxy radicals enhancing the low temperature branching pathways. The activation of this reaction pathway is the major motivation for the relatively high RON and MON indices of alcohol fuels (ethanol, propanol and butanol isomers). As clear from the comparison between panel A and B of Figure 4, its importance decreases with increasing chain length, making longer alcohols (pentanol, hexanol, etc.) gradually more similar to linear alkanes and therefore more suitable for diesel engines or new combustion technologies. The specific low temperature interactions of ethanol α-hydroxyalkyl radical with O_2 have been theoretically investigated by Zádor et al. [54] and by da Silva et al. [55], clearly highlighting in the potential energy surface analysis the low lying pathway leading to the formation of HO_2 and acetaldehyde. Despite a more systematic theoretical evaluation of R-·CH-OH + O_2 for a series of alcohols would be necessary in order to extrapolate meaningful rate rules, the high pressure limit rate constant of da Silva et al. [55], already adopted by Sarathy et al. [5] and Heufer et al. [38], has been corrected accounting for the extra ~4 kcal/mol reported by Zador [54] and co-workers at a higher level of theory. Figure 6 compares such rate constants.

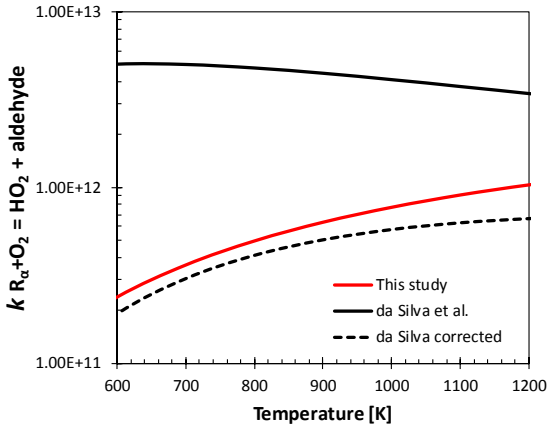

Figure 6: R-·CH-OH+O_2 ↔ R-(C=O)-H+HO_2 high pressure limit rate constant, $k = 4.5\ 10^{12} exp(-3500/RT)$. Units are cm^3, mol, s, cal.

The formation of a carbonyl compound and HO_2 is also considered in successive steps when internal isomerization reactions (RO_2↔QOOH) lead to the formation of a α-hydroxy-hydroperoxyalkyl radical, and its successive interactions with O_2 undergo similar pathways, as summarized in Figure 7.

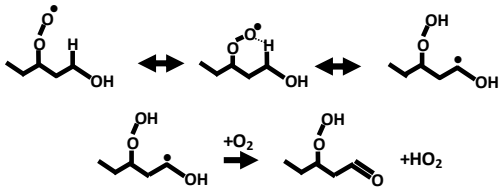

Figure 7: formation of α-hydroxy-hydroperoxyalkyl radical and its interactions with O_2 to form a carbonyl-hydroperoxide (e.g. hydroperoxy pentanal) and HO_2.

The remaining fuel radicals produced by H-abstraction reactions follow the conventional low temperature pathways, whose rate constant are obtained from established alkanes rate rules [44] accounting for the different bond dissociation energies (i.e. C-H in α and β) in isomerization and decomposition steps or from the mechanism of Sarathy [5] (e.g. tautomerization reactions, Waddington reactions etc.). The unconventional dehydration pathway of hydroperoxyalkyl (QOOH) radicals proposed by Welz et al. [56] is also included, and the rate constant is estimated taking into account the formation of a cyclic transition state and the calculated energy barrier (~13 kcal/mol). Further activity should be devoted to obtain a more

accurate kinetic rate constant for this channel, whose steps are reported in **Figure 8**.

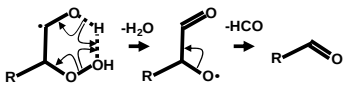

Figure 8: Dehydration channel of QOOH radicals [56] and successive decomposition.

As clearly highlighted in the above discussion and schematically summarized in **Figure 5**, a large amount of aldehydes is produced in alcohols oxidation. In particular the R-·CH-OH+O_2 pathways directly produce the parent aldehydes R-(C=O)-H, whose high and low temperature oxidation have been included according to the work of Pelucchi et al. [57, 58].

The primary reaction in the lumped kinetic mechanism to describe the oxidation of *n*-butanol and *n*-pentanol is reported in Table 3.

Table 3: Kinetic parameters of the lumped oxidation reactions of n-butanol and n-pentanol (units are mol, cm, s, cal).

Lumped reactions	n-butanol			n-pentanol		
	A	***n***	***Ea***	***A***	***n***	***Ea***
R+ O_2 → O_2	7.50E+12	0.0	0	1.00E+13	0.0	0
RO_2 → R + O_2	3.00E+13	0.0	30000	4.00E+13	0.0	30000
RO_2 → Unsat Alcohols + HO_2	0.80E+37	-7.5	39500	1.20E+37	-7.5	39500
RO_2→OH+CH2O+C_{n-1}aldehyde (Waddington)	1.00E+10	0.0	22000	1.00E+10	0.0	22000
RO_2 → QOOH	8.36E+9	0.39	19621.3	2.16E+03	2.463	17204.05
QOOH → RO_2	3.55E+05	1.596	11124.06	5.97E+03	2.186	10839.18
β-QOOH → $H\dot{O}_2$ + Unsat Alcohols	4.04E+07	1.823	23182.1	4.79E+12	0.48	27344.5
γ/δ-QOOH → OH + Olefins	8.19E+15	-1.013	23327.45	1.07E+17	-1.335	23538.5
QOOH → Cyclic Ether + OH	2.78E+10	0.371	17120.7	2.78E+10	0.371	17120.7
QOOH → H_2O + Cn-1 Aldehyde + HCO	3.00E+10	0	13000	3.00E+10	0	13000
QOOH + O_2 → OOQOOH	7.50E+12	0.0	0	1.00E+13	0.0	0
OOQOOH→ QOOH + O_2	3.00E+13	0.0	30000	4.00E+13	0.0	30000
αQOOH + O_2→ $H\dot{O}_2$ + Aldehyde	3.00E+12	0.0	35000	3.00E+12	0.0	35000
OOQOOH → OQOOH + OH	8.36E+9	0.39	19621.3	2.16E+03	2.463	17204.05
OQOOH → OH + Products	9.00E+15	0.0	41500	9.00E+15	0.0	41500

Beyond the kinetic details of Table 3 it is possible to explain the higher reactivity of *n*-pentanol (Figure 2) through some rather simple observations. Beside the higher rate of consumption due to H-abstraction reactions by OH, the longer alkane-like carbon chain allows for enhanced isomerization steps in the low temperature branching pathways, as reported in Figure 9. In particular, Figure 9a shows forward (solid lines) and backward (dashed lines) RO_2↔QOOH isomerization lumped rate constants, whose ratio results in a ~20% higher equilibrium rate constant (Figure 9b) in *n*-pentanol oxidation compared to *n*-butanol.

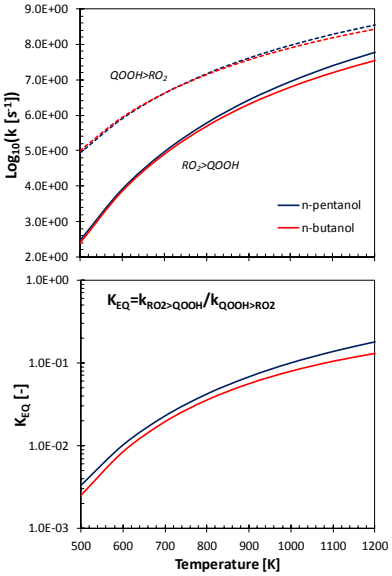

Figure 9: A) RO_2>QOOH (solid lines), QOOH>RO_2 (dashed lines) isomerization rate constants of n-butanol (red) and n-pentanol (blue). B) equilibrium rate constant defined as $k_{RO2>QOOH}/k_{QOOH>RO2}$.

This enhanced isomerization step translates into a more effective low temperature branching for *n*-pentanol, highlighted in terms of normalized ketohydroperoxides mole fraction in Figure 10. The ignition delay time also corresponds to the time at which complete consumption of ketohydroperoxides occurs.

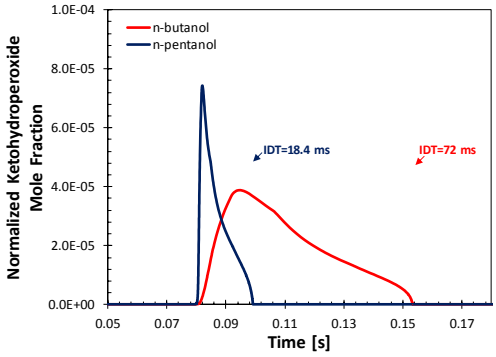

Figure 10: Normalized ketohydroperoxide mole fraction ($x/x_{0,fuel}$) for *n*-butanol and *n*-pentanol stoichiometric mixtures at T_c~830-840 K and P_c~10 bar.

2.3 Kinetic Mechanism Validation

The kinetic mechanism discussed in Section 2.2, has been validated over a wide range of experimental conditions: ignition delay times (T=670-1670 K, p=1-80bar, φ=0.5-2.0), laminar flame speed (p=1 bar, T=343-473 K, φ=0.7-1.7), speciation in jet stirred reactors (T=770-1100 K, p=1-10 bar, φ=0.35-2.0). For sake of brevity only the ignition

delay times are presented and discussed in the following section. Kinetic simulations have been performed using the OpenSMOKE++ framework of Cuoci et al. [59].

Figure 11 compares experimental ignition delay time [60-63] for stoichiometric butanol/O_2/Ar and butanol/air mixtures with kinetic model predictions, over a wide range of temperature and pressures. In a similar way, Figure 12 compares experimental [38, 64, 65] and calculated ignition delay time for n-pentanol. The kinetic mechanism is able to predict temperature and pressure dependence of ignition delay time for both fuels. Maximum deviations for n-butanol are within a factor of ~2 for the RCM data at 10 bar and the shock tube data at 8 bar (Figure 11, blue open squares and black open triangles). n-pentanol predictions systematically deviate from the 9 bar shock tube data [38] (Figure 12 green open diamond). Similar deviations were observed by Heufer et al. [38] and Sarathy et al. [5] (thin green line in Figure 12).

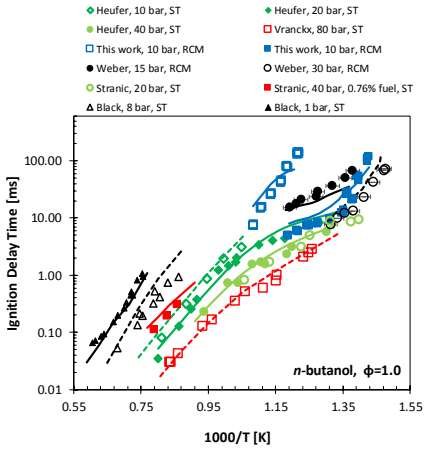

Figure 11: Experimental and simulated ignition delay times of stoichiometric *n*-butanol/O_2/Ar and *n*-butanol/air mixtures.

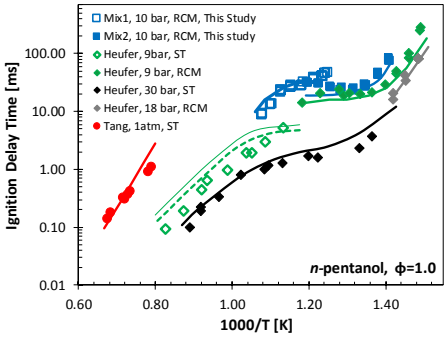

Figure 12: Experimental and simulated ignition delay times of stoichiometric *n*-pentanol/O_2/Ar and *n*-butanol/air mixtures. Thin line: Sarathy et al. mech [5].

Sensitivity analyses have been carried out to investigate the chemistry responsible for the observed ignition trends. Figure *13* compares sensitivity coefficients at p=30 bar and T=650 K for *n*-butanol and *n*-pentanol. As expected from the fundamental similarities between the two alcohols and from the systematic development of the kinetic subsets to describe their combustion, the same hierarchy is observed within the important reaction pathways. The minor differences are due to more or less enhanced low temperature reactivity, resulting from different carbon chain length (i.e. longer alkane-like moiety). The sensitivity coefficients reported in Figure *13* have been scaled assuming a value of -1 for the most inhibiting reaction in both cases (OH+Fuel↔Rα+H_2O). At such temperature the most of the low temperature reactive flux produces ketohydroperoxides (KHYP) whose decomposition provides OH radicals to the H-abstraction reactions. The abstraction on the alkane-like moiety of the molecules largely increases reactivity, allowing the onset of the low temperature branching pathway. To a lesser extent this is also observed for the H-abstraction from the β position. Clearly the H-abstraction from the α-site strongly decreases the reactivity as the only fate of such radical is to produce HO_2 and the corresponding aldehyde.

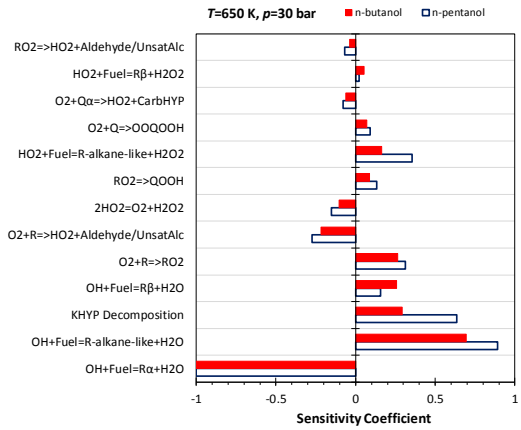

Figure 13: Sensitivity of ignition delay times to rate constants for *n*-butanol-*n*-pentanol/air mixtures at T=650 K and p=30 bar.

Additional interesting insights into the chemistry governing auto-ignition is given in Figure 14, showing the sensitivity coefficient of the most important fuel specific reactions as a function of temperature. For sake of clarity only the *n*-butanol case is reported and discussed, as one should expect analogous observations for *n*-pentanol.

Moving from the lowest temperature condition (T=650 K) already discussed, at T=850 K (blue bars of Figure 14) a rise in the relevance of H-abstractions by HO_2 is observed, despite this H-abstraction by OH still consumes the most of the fuel. HO_2 is mostly produced by H+O_2(+M)↔HO_2(+M), and by HCO+O_2↔CO+HO_2 and by the same interaction of the α radical (Rα) with O_2, discussed above (R-·CH-OH+O_2↔ HO_2+ R-(C=O)-H). It has to be noted that such reaction does not show up in the sensitivity analysis as no alternative pathways exist for Rα. In other words, this channel act as a "sink" of reactivity. H-abstractions by HO_2 directly compete with the termination reaction HO_2+HO_2↔O_2+H_2O_2 strongly inhibiting auto-ignition. The competition between low temperature and intermediate temperature pathways clearly emerges at T=850 K. Observing the high pressure shock tube data of *n*-butanol in Figure 11 it is possible to observe a change of slope around this temperature. This phenomenon becomes even more pronounced in the case of *n*-pentanol, gradually approaching the typical negative temperature coefficient (NTC) behavior of *n*-alkanes. This is due to the increasing importance of alternative decomposition pathways of RO_2 and QOOH radicals and to the direct H-abstraction by O_2 on fuel radicals forming HO_2 and an aldehyde or an unsaturated alcohol (O_2+R→HO_2+Aldehyde/Unsaturated Alcohol). Such alternative channels overcome the low temperature branching, simply propagating the radical chain reaction or, at the limit, inhibiting the reactivity producing less reactive radicals (e.g. HO_2). These statements are

confirmed by the increased sensitivity coefficient of the isomerization reaction $RO_2 \leftrightarrow QOOH$ and of the successive second addition to O_2 ($O_2+QOOH \leftrightarrow OOQOOH$), playing a key role in defining the relative importance of the reactive flux giving branching or propagation.

At higher temperature (T=1200 K), the number of fuel specific reactions which are sensitive to ignition delay time determination largely decreases. In fact, the characteristic time of decomposition of fuel radicals (~10^9 s^{-1}) does not allow for any interaction with molecular oxygen, resulting in dominant role of the C_0-C_2 chemistry.

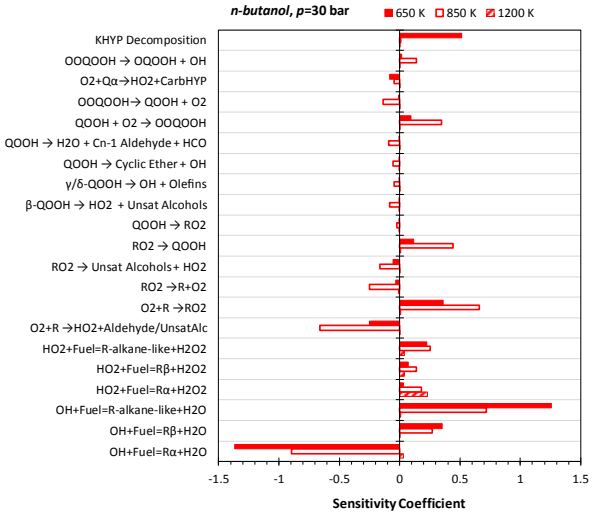

Figure 14: Sensitivity of ignition delay times to rate constants for *n*-butanol /air mixtures p=30 bar and varying temperatures.

Recent experimental and kinetic modelling study focused on PRF and TRF mixtures blended with butanol [33, 40]. As an additional validation target of the proposed *n*-butanol and *n*-pentanol low temperature mechanism, comparison of the POLIMI mechanism with these experimental data are reported in Figure 15 and Figure 16.

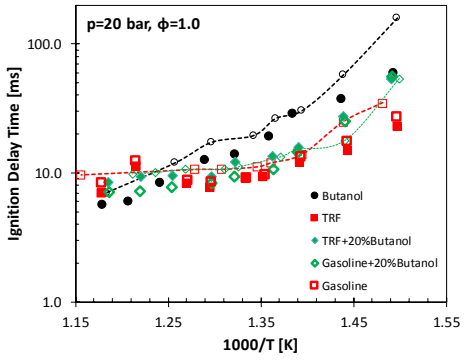

Figure 15: Experimental [33] and simulated ignition delay times for TRF, *n*-butanol, TRF/ *n*-butanol (52.5 % *iso*-octane, 9.1 % *n*-heptane, 18.4 % toluene, 20.0 % *n*-butanol in volume), gasoline and gasoline/*n*-butanol in air mixtures at p=20 bar and φ=1.0.

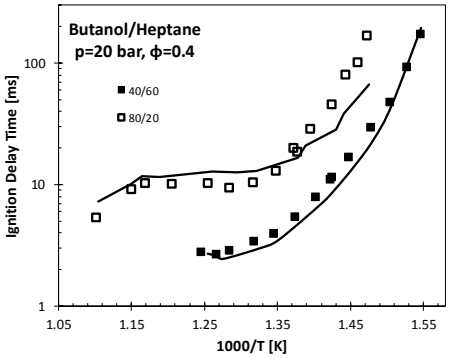

Figure 16: Experimental [40] and simulated ignition delay times for *n*-butanol/ *n*-heptane blends (40/60 and 80/20 in mol %) in air at p=20 bar and φ=0.4.

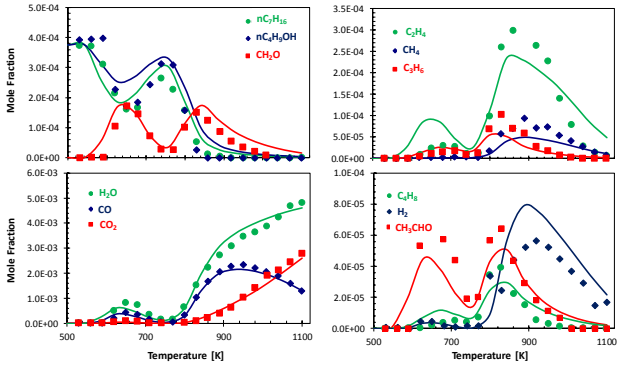

Figure 17: *n*-butanol/ *n*-heptane mixture (50:50) at φ= 0.3, p = 10 atm and τ = 0.7 s. Experimental data (symbols) [66] and model predictions.

3. Multi-zone model of HCCI engine

3.1 Engine Simulation Model

The multi-zone model of HCCI engine developed and validated by Bissoli et al. [32, 67] is briefly reiterated in this Section. **Figure *18*** shows the multi-zone configuration, conceived according to the "*onion-skin*" approach firstly introduced by Komninos et al. [68].

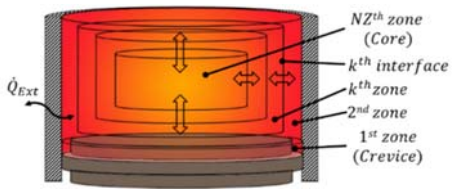

Figure 18: Multi-zone model configuration [32].

The simulation starts at the Intake Valve Closing (IVC) and ends at Exhaust Valve Opening (EVO), therefore it only describes the compression and expansion phases of a four-stroke engine. During each cycle the model evaluates system reactivity in each zone, together with heat and mass exchanged between adjacent zones. The thermal and composition stratification in the charge are accounted for by means of interactions between neighboring zones. A complete and adiabatic mixing between the exhaust gas trapped in the cylinder and the fresh

EGR is assumed. EGR temperature and composition are updated at each cycle, thus affecting the initial conditions of the new cycle.

The different assumptions underlying the model formulation are summarized herein:

1) In-cylinder mixture described as an ideal-gas,
2) Each zone is treated as an ideal reactor with uniform temperature, composition and time-variable volume,
3) Uniform pressure, except for the crevices (constant-volume, variable-mass).

Uniform pressure, except for the crevices (constant-volume, variable-mass).

Details on the heat transfer model, on laminar and turbulent contributions to heat and mass transfer have been discussed in the previous study of Bissoli et al. [32].

The multi-zone model was specifically conceived for simulations with detailed kinetic mechanisms and allows for conventional kinetic analyses such as Sensitivity Analysis and Rate of Production Analysis.

The validation of the model was previously reported for *n*-heptane, *n*-butanol, and methyl-esters [32] (*+Energy & Fuels, 2017, Submitted*). The multi-zone model was able to properly reproduce compression and expansion phases, pressure peak and the combustion phasing. Moreover, very good predictions of reactivity and emissions were obtained, based on CO, CO_2 and other intermediate species (aldehydes) profiles as a function of the compression ratio (CR).

The recent work of Bissoli et al. (*Energy & Fuels, 2017, Submitted*) focused on the experimental measurements obtained in a Ricardo E6 engine at Brunel University [69] for PRF80, PRF100 and ethanol. For the sake of comparison, the simulations performed in this study are carried out in the same engine configuration. Engine characteristics and specific model parameters are reported in Table 4. These parameters were obtained by performing simulations using 15 zones, with a crevice volume equal to 2% of the clearance volume. As already discussed [32], such number of zones constitutes a good compromise between computational efforts and the detailed description of the phenomena involved.

Table 4: Ricardo E6 [69]. Engine characteristic and specific model parameters.

Displacement [cm^3]	504	Speed [rpm]	1500
Bore [mm]	76.2	Intake Valve Closing [°ATDC]	137
Stroke [mm]	111.1	Exhaust Valve Opening [°BTDC]	144
Rod Length [mm]	241.3	Cu_z	0.12
Compression Ratio	11.5	Cu_w	0.58

3.2 Operability and performance maps of HCCI engines

Oakley and co-workers [69, 70] systematically explored the air-fuel ratio (AFR) versus EGR operating range of the Ricardo E6 single-cylinder engine at fixed speed and compression ratio (CR) for different fuels. Three zones limiting the stability of HCCI regime were identified: the first one at low loads, called partial burn, characterized by low engine efficiencies; the knocking region, observed at high loads, where high pressure rise rates occur, and the misfire zone, at high dilutions, where high cycle-to-cycle variations are registered. Figure 19 shows a typical operative map for a HCCI engine.

The features of these three different combustion regimes are highlighted in Figure 20. High loads (low λ) and low EGR cause the ringing phenomena, characterized by a strong PRR. Partial burn is characterized by an incomplete combustion, with consequent reduction of combustion efficiency (η_{comb}), defined as:

$$\eta_{comb} = \frac{\int HRR}{\Delta H_{combustion}}$$

Misfire is observed at high EGR dilutions and represents an unstable condition, where the engine goes towards periodical oscillations. This regime is characterized by strong increases in cycle-to-cycle variability, quantified in terms of variation of the indicated mean pressure (CoV IMEP) defined as:

$$\text{CoV IMEP} = \frac{\sigma_{IMEP}}{IMEP}$$

where the IMEP is calculated as:

$$\text{IMEP} = \frac{\int pdV}{V_{disp}}$$

and σ_{IMEP} is its standard deviation.

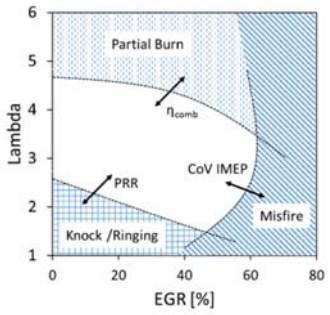

Figure 19: Typical λ-EGR operative map of a HCCI engine, together with critical limits of different combustion regions. Adapted from Bissoli et al. (Energy & Fuels, 2017, Submitted).

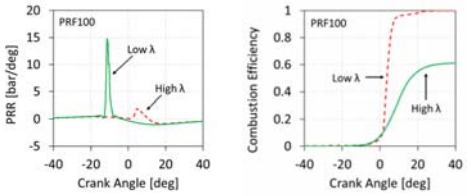

Ringing *Partial Burn*

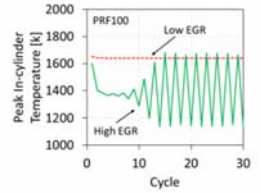

Misfire

Figure 20: Qualitative visualization of critical conditions limiting the operability of HCCI engines. Adapted from Bissoli et al. (Energy & Fuels, 2017, Submitted).

The operability maps presented in this study are generated by independently varying the EGR ratio (mass-basis) and λ, considered as the global in-cylinder air-to-fuel ratio (AFR) after mixing EGR with the fresh feed. For each map more than 150 EGR and λ combinations are investigated, with 50 simulation cycles for each point to account for the EGR cycle-cycle variability. Different characteristics such as ignition timing, indicated mean effective pressure (IMEP) and exhaust emission are plotted inside the different maps averaging the last 10 simulation cycles. The limits of the stable combustion region are defined as the set of λ-EGR satisfying the requirement of $\eta_{comb} \geq 80\%$, CoV IMEP $\leq 60\%$ and PRR ≤ 6 bar/deg. Such threshold values are deduced from the experimental study of Oakley [69] and are comparable with those adopted in other studies [71, 72].

4. Results and Discussion

Figure 21 compares the predicted HCCI operating regions for the investigated fuels. Ethanol and the TRF/butanol mixture [33] representative of a PR5801 gasoline (RON=95, MON=86.6), slightly extend the operability map toward the ringing region, due to the presence of highly anti-knocking components such as ethanol, iso-octane and toluene. *n*-pentanol instead shows a trend which is more similar to PRF100, with butanol lying in between. As previously observed *(Energy & Fuels, 2017, Submitted),* ringing phenomena are scarcely affected by the fuel type. *n*-butanol and *n*-pentanol show the highest flexibility to both EGR dilution and engine load, with the TRF/butanol surrogate showing a behavior in between ethanol and PRFs mixtures.

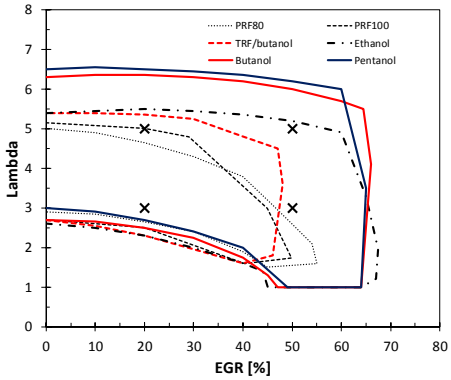

Figure 21: Comparison of predicted HCCI operating limits for the different fuels. Ethanol, PRF80 and PRF100 adapted from Bissoli et al. (Energy & Fuels, 2017, Submitted). Symbols are the operating conditions at which the kinetic features of the system are compared between the different fuels.

Figure 22 and *Figure 23* exemplify the behavior of the different classes of fuels discussed in this paper, by comparing the performance of PRF80 with the TRF/butanol mixture. As expected, Figure 22 shows that engine load increases when air and EGR ratios decrease, since stoichiometric and undiluted conditions are approached. Both fuels have similar trends in the whole range, with also similar peak values of ~2.5 bar. TRF mixture shows a wider stability, allowing to reach stable combustion at lower loads (~1 bar).

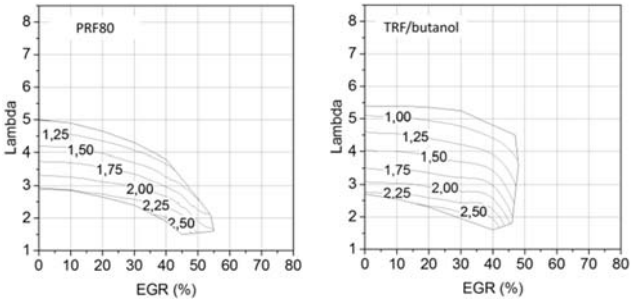

Figure 22: Engine load maps reported as IMEP [bar]. Comparison between PRF80 and TRF/butanol mixture.

A similar behavior is observed for the indicated thermal efficiency in Figure 23. PRF80 and TRF/butanol mixtures shows very similar trends, with efficiency increasing with fuel amount in the intake charge. On the contrary, air dilution and large EGR ratios reduce it. Both fuels show that thermal efficiency ranges from ~30% to ~36%, with TRF/butanol mixture showing a slightly large lower limit of efficiency (~28%), related with the larger operating region close to partial burn conditions.

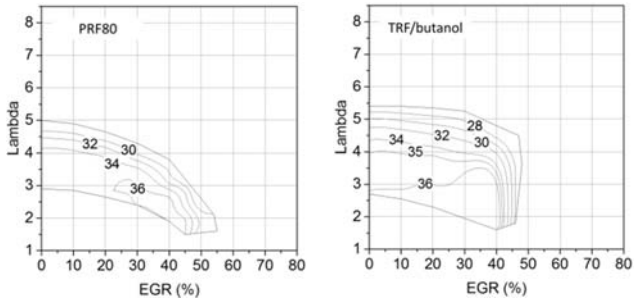

Figure 23: Indicated thermal efficiency maps [%]. Comparison between PRF80 and TRF/butanol mixture.

The reason behind the large stability region of *n*-butanol and *n*-pentanol have to be referred to their ignition propensity. Beside the kinetic features of long chain alcohols, already discussed in Section 2, *Figure 24* shows the effect of engine load and EGR on ethanol and *n*-pentanol constant volume batch reactor ignition delay times.

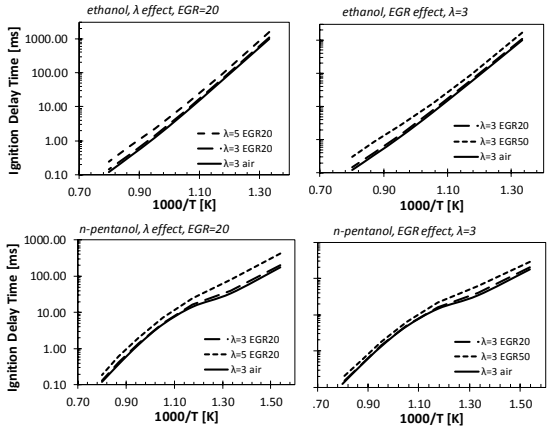

Figure 24: Load and EGR effect on ethanol and *n*-pentanol ignition delay times. Constant volume batch reactor simulations, p=20 bar.

Similar responses for ethanol and *n*-pentanol are observed for varying EGR dilution (right panels) at low temperatures (T<900 K), justifying the very similar stability limits toward the misfire region. *n*-pentanol is much more sensitive to load variation (left panels), in particular at low temperatures, resulting in wider limits at low loads (high λ, lower fuel concentration). Sensitivity analysis from the multi-zone model allows to better understand such trends. Figure *25* compares the sensitivity coefficient of ethanol, n-butanol and n-pentanol at λ~5 and EGR=20%. As already discussed by Bissoli et al. (*Energy & Fuels, 2017, Submitted*) ethanol chemistry is dominated by hydrogen peroxide (H_2O_2) and hydroperoxy radical chemistry (HO_2). The lack of a significant alkane-like moiety typical of longer alcohols, prevents any low temperature reactivity, resulting in extremely high yields of HO_2, mostly formed by the interaction of the α radical (Rα, CH_3-CH-OH) with O_2, producing acetaldehyde. As reported in Figure *25*, the typical low temperature reactions emerge as strongly sensitive for *n*-butanol and *n*-pentanol. The availability of such pathways, results in higher yields of OH, sustaining the reactivity (shorter ignition delay times, Figure *26*) and enlarging heavier alcohols operability maps. These statements are confirmed by the sensitivity diagram. Moreover, comparable sensitivity coefficients are observed for $HO_2+HO_2=O_2+H_2O_2$ and for H_2O_2 (+M) = 2OH(+M) for the different fuels, while butanol and pentanol are more sensitive to H-abstraction reactions by OH, whose concentration is sustained by the low temperature branching.

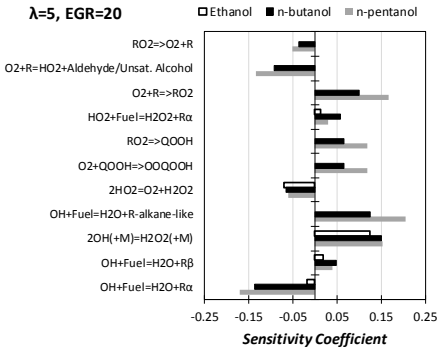

Figure 25: Sensitivity analysis of the temperature in the inner zone for different fuels at λ=5 and EGR=20%. A positive sensitivity coefficient stands for a reaction increasing reactivity.

The addition of butanol to the TRF mixture investigated by Agbro et al. [33] is responsible for the extension of the stable region toward lower loads. Ignition delay times at λ~5 and EGR=20% have been calculated for such mixture and are compared with those of ethanol, *n*-butanol and *n*-pentanol in Figure *26*.

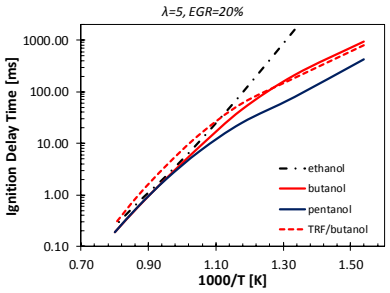

Figure 26: Ignition delay times of the different fuels at λ~5 and EGR=20 %, p=20 bar.

The TRF/butanol mixture is the slowest to ignite for T>900 K, while at low temperatures it behaves very similarly to n-butanol. These observations justify both the slightly narrower ringing region overlapping ethanol, and the lower loads at which the HCCI engine can operate with respect to PRF80 and PRF 100. To better investigate the acting chemistry, and the kinetic influence of *n*-butanol, sensitivity analyses have been carried out at both T=850 K and T=1150 K (Figure *27*).

At the lowest temperatures the reactivity is dominated by H-abstraction by OH from *n*-butanol, producing Rα. *n*-heptane and *iso*-octane low temperature reactions rule the ignition propensity, together with H-abstraction from the alkane-like moiety of *n*-butanol. At higher temperatures (T=1150 K) the reactivity is dominated by reactions belonging to the core C_0-C_2 mechanism, together with the unimolecular intiation of *iso*-octane, the most abundant component in the fuel mixture, responsible for the overall radical chain initiation. Such intiation involves the formation of alkyl radicals such as iso-propyl (iC_3H_7), iso-butyl, tert-butyl and neo-pentyl radical, whose successive decomposition reactions produce methyl radical and unsaturated species (C_3H_6, iso-C_4H_8), sequentially leading to the formation of resonance-stabilized radicals (allyl, methylallyl). The abundance of the primary C-H site available for H-abstraction also justifies the lower ignitability of *iso*-octane at high temperatures.

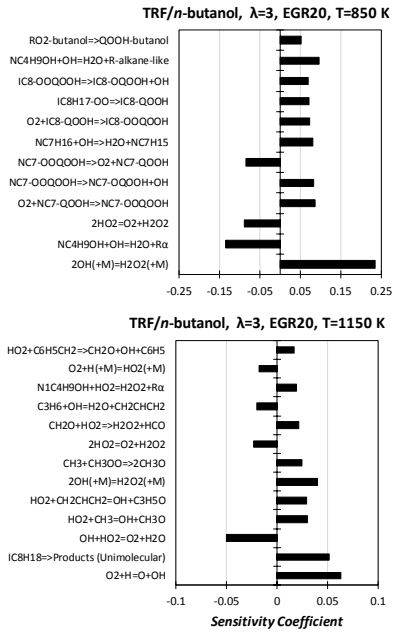

Figure 27: Sensitivity analysis of the ignition delay times to reaction rate constants at p=20 bar. Constant volume batch reactor simulation.

Figure *28* shows predicted pressure traces at different dilutions and EGR ratios for *n*-butanol, *n*-pentanol and TRF/*n*-butanol mixture. Pressure traces at similar conditions (EGR=20, λ~3) for the different fuels are also compared in the bottom right panel. Higher EGR (EGR=50) and lower loads (λ~5) result in a smoother transition to the hot ignition in the case of alcohols, as highlighted by the different first derivatives at the inflection point (CAD ~-4.1 deg). The following analysis focuses on the two limiting cases: the high EGR dilution and low loads (EGR50, λ=5) and the low EGR dilution and high loads (EGR20, λ=3). Sensitivity analyses have been performed at the conditions of temperature, pressure and mixture composition marked by the black crosses in Figure *28*, to investigate the relevant kinetics. Figure *29* and Figure *30* show the results.

Starting from the lower temperature, lower pressure cases (CAD=-30, T~900 K, p~9 bar) both mixtures are largely dominated by HO_2 chemistry, similarly to what observed for the cases of Figure *24*. Namely, the reactivity is strongly inhibited by the termination step $HO_2+HO_2=O_2+H_2O_2$ and enhanced by hydrogen peroxide decomposition (H_2O_2 (+M)=2OH(+M)). The reactivity is also strongly enhanced by H-abstractions by HO_2 from the weak C-H bond in α. In fact, this channel provides a large amount of H_2O_2, whose decomposition rules the reactivity. The importance of the correct definition of the relative weight of the channels involving QOOH (i.e. second addition to O_2, decomposition to HO_2 and unsaturated alcohols, backward isomerization to RO_2 etc.) are also highlighted in Figure *29*. The intermediate temperature conditions move the focal point of the kinetics toward species preceding ketohydroperoxides formation (QOOH, OOQOOH). Once again, the relative selectivity of H-abstraction by OH from the different carbon site plays a major role.

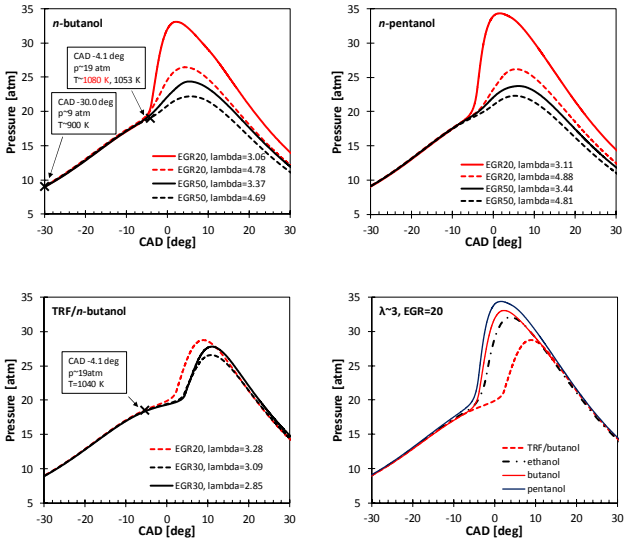

Figure 28: Pressure traces calculated at varying λ and EGR dilution for *n*-butanol, *n*-pentanol and the TRF/*n*-butanol mixture.

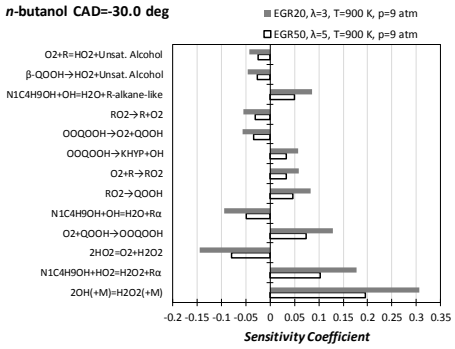

Figure 29: Sensitivity analysis at CAD=-30.0, for the EGR20 λ=3 and EGR50 λ=5 cases.

Figure *30* highlights the important reactions at the inflection point, characterizing the transition to hot ignition. H-abstraction by HO_2 at the α position becomes the most important reaction in enhancing reactivity. Differently from what previously discussed for OH, where the H-abstraction from the same site generally reduces the reactivity, the direct formation of H_2O_2 associated with H-abstractions by HO_2 has a positive effect of reactivity. This is due to the extreme relevance of hydrogen peroxide decomposition: the formation of Rα, further propagates the reactivity producing additional HO_2 through the same interaction discussed above (R-·CH-OH+O_2↔ HO_2+ R-(C=O)-H**).**

Concerning the higher first derivative at the inflection point observed for the EGR20 λ=3 case, this is mostly due to a higher concentration of fuel radical in the inlet charge, speeding up fuel decomposition thus providing higher yields of radical species, including Rα.

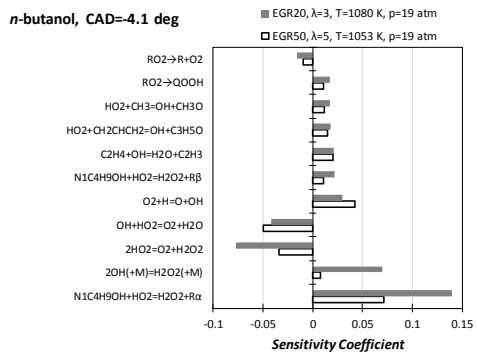

Figure 30: Sensitivity analysis at CAD=-4.1, for the EGR20 λ=3 and EGR50 λ=5 cases.

The ignition of the TRF/butanol mixture is delayed of ~10 CAD. From a kinetic perspective, as previously discussed at the same EGR and λ conditions in Figure *27*, this has to be referred to the lower reactivity of iso-octane and toluene.

Figure *31* compares predicted formaldehyde (CH_2O) and CO emissions for PRF80 and the TRF/butanol surrogates. CH_2O and CO are typical pollutants largely released when incomplete combustion phenomena occur. PRF80 produces higher emissions of formaldehyde, found to be a factor of ~2-5 higher considering the same load and EGR conditions. Also CO emissions are higher of a factor of ~2-3 in the case of PRF80. In general formaldehyde and CO emissions increase for decreasing load and increasing EGR dilution. This phenomena is largely motivated by the decreasing thermal efficiency (Figure *23*), typically observed when moving toward leaner and more diluted conditions.

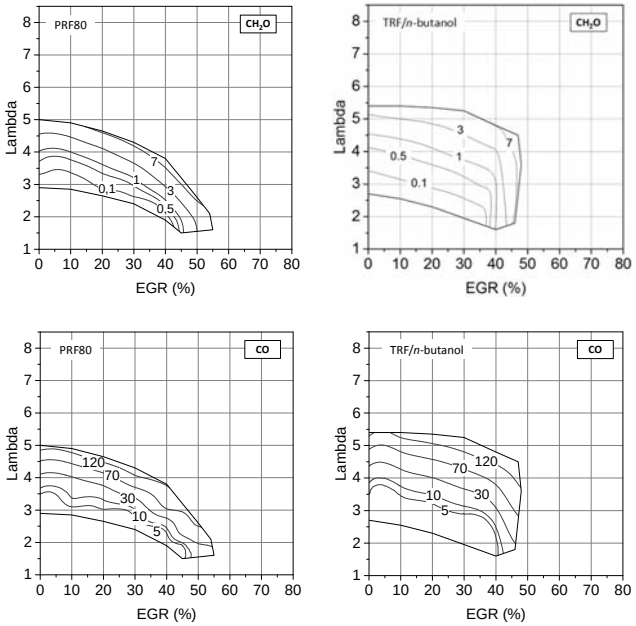

Figure 31: Maps of CH_2O and CO exhaust emissions [g/kWh]. Comparison between PRF80 and TRF/butanol mixture.

At low temperatures, CH_2O directly derives from ketohydroperoxides decomposition. Moving toward higher temperatures, CH_2O production is ruled by interactions of HO_2 and CH_3 radicals producing methoxy radical (CH_3O) through the reaction $HO_2+CH_3 \leftrightarrow CH_3O+OH$. The further dehydrogenation of CH_3O largely explains CH_2O production. The larger HO_2 yields previously mentioned in the case of *n*-butanol addition, result in an enhanced $HO_2+HO_2=O_2+H_2O_2$ channel, partly limiting formaldehyde formation. Further oxidative steps of formaldehyde involve the H-abstraction producing formyl radical (HCO), rapidly decomposed to produce CO.

5. Conclusions

A systematic experimental analysis of linear C_2-C_5 alcohols ignition delay time at high pressure (10-30 bar) and low temperatures 700-925 K, allowed the revision of the POLIMI mechanism for alcohols oxidation. Firstly, this study presented and discussed the new experimental measurements for *n*-butanol and *n*-pentanol. The development of the kinetic mechanism is then discussed focusing on alcohol-specific reaction pathways in the low and intermediate temperature oxidation regime. Model comparison with a wide set of ignition delay time measurements from this and from previous studies proves reliability of the proposed kinetic model. Following the recent trends of fuel formulation, requiring the blending of biofuels such as alcohols to conventional hydrocarbon fuels, the kinetic model is also compared to PRF and TRF/*n*-butanol mixtures, further confirming the validity of the alcohol sub-mechanism. A broad kinetic discussion serves the goal of characterizing the ignition propensity of such fuels, highlighting key reaction steps.

The HCCI multi-zone model of Bissoli et al. [32], widely validated and recently used to highlight the promising performances of ethanol (*Energy & Fuels, 2017, submitted*), was used to investigate the operability maps of *n*-butanol, *n*-pentanol and the same TRF/*n*-butanol mixture, focusing on the kinetic features governing the performances of such fuels in HCCI engine. *n*-butanol and *n*-pentanol extend the operability maps of ethanol even further, mostly in terms of allowing lower loads, thus reducing the partial-burn region. Similarly, the addition of *n*-butanol to a TRF mixture representative of a PR5801 gasoline, significantly impacts the ignition chemistry, slightly extending the operating limits of PRF100 and PRF80 previously analyzed by Bissoli et al. (*Energy & Fuels, 2017, submitted*).

From a chemical kinetics perspective, an alcohol molecule can be divided into two moieties. The first one, alcohols specific, is strongly influenced by the presence of the hydroxyl moiety (R-OH), influencing C-H and C-C bond strengths and largely preventing alkane-like low temperature branching pathways as discussed in Section 2. The oxidation of the remaining moiety instead proceeds according to conventional pathways. Therefore, the longer the alkane-like portion the closer the C_n alcohol ignition propensity to that of the C_n alkane. As discussed by Pelucchi et al. [37] and by Heufer et al. [38] these chemical and kinetic features translate into a higher reactivity at higher temperatures and a lower reactivity at lower temperatures, when comparing alcohols with the homologous alkanes.

References

[1] Exxonmobil, The Outlook for Energy: A View to 2040, 2015.

[2] C2ES, Outcomes of the UN climate change conference in Paris. http://www.c2es.org/docUploads/cop-21-paris-summary-02-2016-final.pdf.

[3] L. Coniglio, H. Bennadji, P.A. Glaude, O. Herbinet, F. Billaud, Combustion chemical kinetics of biodiesel and related compounds (methyl and ethyl esters): experiments and modeling–advances and future refinements, Progress in Energy and Combustion Science 39 (2013) 340-382.

[4] M. Shahabuddin, A. Liaquat, H. Masjuki, M. Kalam, M. Mofijur, Ignition delay, combustion and emission characteristics of diesel engine fueled with biodiesel, Renewable and Sustainable Energy Reviews 21 (2013) 623-632.

[5] S.M. Sarathy, P. Oßwald, N. Hansen, K. Kohse-Höinghaus, Alcohol combustion chemistry, Progress in Energy and Combustion Science 44 (2014) 40-102.

[6] A. Sudholt, L. Cai, J. Heyne, F.M. Haas, H. Pitsch, F.L. Dryer, Ignition characteristics of a bio-derived class of saturated and unsaturated furans for engine applications, Proceedings of the Combustion Institute 35 (2015) 2957-2965.

[7] S. Atsumi, T. Hanai, J.C. Liao, Non-fermentative pathways for synthesis of branched-chain higher alcohols as biofuels, Nature 451 (2008) 86-89.

[8] P.P. Peralta-Yahya, J.D. Keasling, Advanced biofuel production in microbes, Biotechnology journal 5 (2010) 147-162.

[9] EPA, Federal Register Environmental Protection Agency Federal Register, 2012.

[10] D. Rakopoulos, C. Rakopoulos, E. Giakoumis, A. Dimaratos, D. Kyritsis, Effects of butanol–diesel fuel blends on the performance and emissions of a high-speed DI diesel engine, Energy Conversion and Management 51 (2010) 1989-1997.

[11] L. Siwale, L. Kristóf, T. Adam, A. Bereczky, M. Mbarawa, A. Penninger, A. Kolesnikov, Combustion and emission characteristics of n-butanol/diesel fuel blend in a turbo-charged compression ignition engine, Fuel 107 (2013) 409-418.

[12] G. Valentino, F.E. Corcione, S.E. Iannuzzi, S. Serra, Experimental study on performance and emissions of a high speed diesel engine fuelled with n-butanol diesel blends under premixed low temperature combustion, Fuel 92 (2012) 295-307.

[13] J. Campos-Fernandez, J.M. Arnal, J. Gomez, N. Lacalle, M.P. Dorado, Performance tests of a diesel engine fueled with pentanol/diesel fuel blends, Fuel 107 (2013) 866-872.

[14] L. Wei, C. Cheung, Z. Huang, Effect of n-pentanol addition on the combustion, performance and emission characteristics of a direct-injection diesel engine, Energy 70 (2014) 172-180.

[15] L. Li, J. Wang, Z. Wang, J. Xiao, Combustion and emission characteristics of diesel engine fueled with diesel/biodiesel/pentanol fuel blends, Fuel 156 (2015) 211-218.

[16] G.T. Kalghatgi, The outlook for fuels for internal combustion engines, International Journal of Engine Research, (2014) 1468087414526189.

[17] J.M. Bergthorson, M.J. Thomson, A review of the combustion and emissions properties of advanced transportation biofuels and their impact on existing and future engines, Renewable and Sustainable Energy Reviews 42 (2015) 1393-1417.

[18] N. Morgan, A. Smallbone, A. Bhave, M. Kraft, R. Cracknell, G. Kalghatgi, Mapping surrogate gasoline compositions into RON/MON space, Combustion and Flame 157 (2010) 1122-1131.

[19] M. Yao, Z. Zheng, H. Liu, Progress and recent trends in homogeneous charge compression ignition (HCCI) engines, Progress in Energy and Combustion Science 35 (2009) 398-437.

[20] K. Epping, S. Aceves, R. Bechtold, J.E. Dec, The potential of HCCI combustion for high efficiency and low emissions, Report No. 0148-7191, SAE Technical Paper, 2002.

[21] N. Komninos, C. Rakopoulos, Modeling HCCI combustion of biofuels: A review, Renewable and Sustainable Energy Reviews 16 (2012) 1588-1610.

[22] M.-B. Liu, B.-Q. He, H. Zhao, Effect of air dilution and effective compression ratio on the combustion characteristics of a HCCI (homogeneous charge compression ignition) engine fuelled with n-butanol, Energy 85 (2015) 296-303.

[23] X. Han, M. Wang, M. Zheng, An enabling study of neat n-butanol HCCI combustion on a high compression-ratio diesel engine, Report No. 0148-7191, SAE Technical Paper, 2015.

[24] K. Xie, T. Yanai, Z. Yang, G. Reader, M. Zheng, Emission Analysis of HCCI Combustion in a Diesel Engine Fueled by Butanol, Report No. 0148-7191, SAE Technical Paper, 2016.

[25] J.H. Mack, D. Schuler, R.H. Butt, R.W. Dibble, Experimental investigation of butanol isomer combustion in Homogeneous Charge Compression Ignition (HCCI) engines, Applied Energy 165 (2016) 612-626.

[26] J. Martinez-Frias, S.M. Aceves, D. Flowers, J.R. Smith, R. Dibble, HCCI engine control by thermal management, Report No. 0148-7191, SAE Technical Paper, 2000.

[27] P.E. Yelvington, W.H. Green, Prediction of the knock limit and viable operating range for a homogeneous-charge compression-ignition (HCCI) engine, Report No. 0148-7191, SAE Technical paper, 2003.

[28] Y. Yang, J.E. Dec, N. Dronniou, M. Sjöberg, W. Cannella, Partial fuel stratification to control HCCI heat release rates: fuel composition and other factors affecting pre-ignition reactions of two-stage ignition fuels, SAE International Journal of Engines 4 (2011) 1903-1920.

[29] H. Aichlmayr, D. Kittelson, M. Zachariah, Miniature free-piston homogeneous charge compression ignition engine-compressor concept—Part II: modeling HCCI combustion in small scales with detailed homogeneous gas phase chemical kinetics, Chemical Engineering Science 57 (2002) 4173-4186.

[30] A. Pinheiro, D. Vuilleumier, D. Kozarac, S. Saxena, Simulating a complete performance map of an ethanol-fueled boosted HCCI engine, Report No. 0148-7191, SAE Technical Paper, 2015.

[31] E. Ortiz-Soto, D. Assanis, A. Babajimopoulos, A comprehensive engine to drive-cycle modelling framework for the fuel economy assessment of advanced engine and combustion technologies, International Journal of Engine Research 13 (2012) 287-304.

[32] M. Bissoli, A. Frassoldati, A. Cuoci, E. Ranzi, M. Mehl, T. Faravelli, A new predictive multi-zone model for HCCI engine combustion, Applied Energy 178 (2016) 826-843.

[33] E. Agbro, A.S. Tomlin, M. Lawes, S. Park, S.M. Sarathy, The influence of n-butanol blending on the ignition delay times of gasoline and its surrogate at high pressures, Fuel 187 (2017) 211-219.

[34] A. Frassoldati, A. Cuoci, T. Faravelli, U. Niemann, E. Ranzi, R. Seiser, K. Seshadri, An experimental and kinetic modeling study of n-propanol and iso-propanol combustion, Combustion and Flame 157 (2010) 2-16.

[35] R. Grana, A. Frassoldati, T. Faravelli, U. Niemann, E. Ranzi, R. Seiser, R. Cattolica, K. Seshadri, An experimental and kinetic modeling study of combustion of isomers of butanol, Combustion and Flame 157 (2010) 2137-2154.

[36] D. Nativel, M. Pelucchi, A. Frassoldati, A. Comandini, A. Cuoci, E. Ranzi, N. Chaumeix, T. Faravelli, Laminar flame speeds of pentanol isomers: An experimental and modeling study, Combustion and Flame 166 (2016) 1-18.

[37] M. Pelucchi, C. Cavallotti, E. Ranzi, A. Frassoldati, T. Faravelli, Relative Reactivity of Oxygenated Fuels: Alcohols, Aldehydes, Ketones, and Methyl Esters, Energy & Fuels 30 (2016) 8665-8679.

[38] K.A. Heufer, S.M. Sarathy, H.J. Curran, A.C. Davis, C.K. Westbrook, W.J. Pitz, Detailed kinetic modeling study of n-pentanol oxidation, Energy & Fuels 26 (2012) 6678-6685.

[39] H.-H. Carstensen, A.M. Dean, Development of detailed kinetic models for the thermal conversion of biomass via first principle methods and rate estimation rules, Computational Modeling in Lignocellulosic Biofuel Production, Oxford University Press, Oxford, UK 201 (2010).

[40] K. Kumar, Y. Zhang, C.-J. Sung, W.J. Pitz, Autoignition response of n-butanol and its blends with primary reference fuel constituents of gasoline, Combustion and Flame 162 (2015) 2466-2479.

[41] E. Ranzi, A. Frassoldati, A. Stagni, M. Pelucchi, A. Cuoci, T. Faravelli, Reduced kinetic schemes of complex reaction systems: fossil and biomass-derived transportation fuels, International Journal of Chemical Kinetics 46 (2014) 512-542.

[42] M. Pelucchi, M. Bissoli, C. Cavallotti, A. Cuoci, T. Faravelli, A. Frassoldati, E. Ranzi, A. Stagni, Improved kinetic model of the low-temperature oxidation of n-heptane, Energy & Fuels 28 (2014) 7178-7193.

[43] M. Pelucchi, Development of Kinetic Mechanisms for the Combustion of Renewable Fuels, Department of Chemistry, Materials and Chemical Engineering "G. Natta", Politecnico di Milano, 2017, pp. 406.

[44] E. Ranzi, M. Dente, A. Goldaniga, G. Bozzano, T. Faravelli, Lumping procedures in detailed kinetic modeling of gasification, pyrolysis, partial oxidation and combustion of hydrocarbon mixtures, Progress in Energy and Combustion Science 27 (2001) 99-139.

[45] E. Ranzi, A. Frassoldati, S. Granata, T. Faravelli, Wide-range kinetic modeling study of the pyrolysis, partial oxidation, and combustion of heavy n-alkanes, Industrial & engineering chemistry research 44 (2005) 5170-5183.

[46] D. Darcy, H. Nakamura, C. Tobin, M. Mehl, W. Metcalfe, W. Pitz, C. Westbrook, H. Curran, A high-pressure rapid compression machine study of n-propylbenzene ignition, Combustion and Flame 161 (2014) 65-74.

[47] S. Burke, J. Simmie, H. Curran, Critical Evaluation of Thermochemical Properties of C1–C4 Species: Updated Group-Contributions to Estimate Thermochemical Properties, Journal of Physical and Chemical Reference Data 44 (2015) 013101.

[48] C.-W. Zhou, J.M. Simmie, H.J. Curran, Rate constants for hydrogen-abstraction by from n-butanol, Combustion and Flame 158 (2011) 726-731.

[49] C.W. Zhou, J.M. Simmie, H.J. Curran, Rate constants for hydrogen abstraction by HȮ2 from n-butanol, International Journal of Chemical Kinetics 44 (2012) 155-164.

[50] D. Katsikadakos, C.-W. Zhou, J. Simmie, H. Curran, P. Hunt, Y. Hardalupas, A. Taylor, Rate constants of hydrogen abstraction by methyl radical from n-butanol and a comparison of CanTherm, MultiWell and Variflex, Proceedings of the Combustion Institute 34 (2013) 483-491.

[51] E. Ranzi, M. Dente, T. Faravelli, G. Pennati, Prediction of kinetic parameters for hydrogen abstraction reactions, Combustion science and technology 95 (1993) 1-50.

[52] H. Curran, Rate constant estimation for C1 to C4 alkyl and alkoxyl radical decomposition, International journal of chemical kinetics 38 (2006) 250-275.

[53] H. Curran, P. Gaffuri, W.J. Pitz, C.K. Westbrook, A comprehensive modeling study of n-heptane oxidation, Combustion and flame 114 (1998) 149-177.

[54] J. Zádor, R.X. Fernandes, Y. Georgievskii, G. Meloni, C.A. Taatjes, J.A. Miller, The reaction of hydroxyethyl radicals with O 2: A theoretical analysis and experimental product study, Proceedings of the Combustion Institute 32 (2009) 271-277.

[55] G. da Silva, J.W. Bozzelli, L. Liang, J.T. Farrell, Ethanol oxidation: Kinetics of the α-hydroxyethyl radical+ O2 reaction, The Journal of Physical Chemistry A 113 (2009) 8923-8933.

[56] O. Welz, S.J. Klippenstein, L.B. Harding, C.A. Taatjes, J. Zádor, Unconventional peroxy chemistry in alcohol oxidation: the water elimination pathway, The journal of physical chemistry letters 4 (2013) 350-354.

[57] M. Pelucchi, E. Ranzi, A. Frassoldati, T. Faravelli, Alkyl radicals rule the low temperature oxidation of long chain aldehydes, Proceedings of the Combustion Institute, (2016).

[58] M. Pelucchi, K.P. Somers, K. Yasunaga, U. Burke, A. Frassoldati, E. Ranzi, H.J. Curran, T. Faravelli, An experimental and kinetic modeling study of the pyrolysis and oxidation of n-C 3 C 5 aldehydes in shock tubes, Combustion and Flame 162 (2015) 265-286.

[59] A. Cuoci, A. Frassoldati, T. Faravelli, E. Ranzi, OpenSMOKE++: An object-oriented framework for the numerical modeling of reactive systems with detailed kinetic mechanisms, Computer Physics Communications 192 (2015) 237-264.

[60] S. Vranckx, K. Heufer, C. Lee, H. Olivier, L. Schill, W. Kopp, K. Leonhard, C. Taatjes, R. Fernandes, Role of peroxy chemistry in the high-pressure ignition of n-butanol–Experiments and detailed kinetic modelling, combustion and flame 158 (2011) 1444-1455.

[61] B.W. Weber, K. Kumar, Y. Zhang, C.-J. Sung, Autoignition of n-butanol at elevated pressure and low-to-intermediate temperature, Combustion and Flame 158 (2011) 809-819.

[62] G. Black, H.J. Curran, S. Pichon, J.M. Simmie, V. Zhukov, Bio-butanol: Combustion properties and detailed chemical kinetic model, Combustion and Flame 157 (2010) 363-373.

[63] I. Stranic, D.P. Chase, J.T. Harmon, S. Yang, D.F. Davidson, R.K. Hanson, Shock tube measurements of ignition delay times for the butanol isomers, Combustion and Flame 159 (2012) 516-527.

[64] K. Heufer, J. Bugler, H. Curran, A comparison of longer alkane and alcohol ignition including new experimental results for n-pentanol and n-hexanol, Proceedings of the Combustion Institute 34 (2013) 511-518.

[65] C. Tang, L. Wei, X. Man, J. Zhang, Z. Huang, C.K. Law, High temperature ignition delay times of C5 primary alcohols, Combustion and Flame 160 (2013) 520-529.

[66] P. Dagaut, C. Togbé, Experimental and modeling study of the kinetics of oxidation of butanol− n-heptane mixtures in a jet-stirred reactor, Energy & Fuels 23 (2009) 3527-3535.

[67] M. Bissoli, A. Cuoci, A. Frassoldati, T. Faravelli, E. Ranzi, T. Lucchini, G. D'Errico, F. Contino, Detailed Kinetic Analysis of HCCI Combustion Using a New Multi-Zone Model and CFD Simulations, SAE International Journal of Engines 6 (2013) 1594-1609.

[68] N. Komninos, D. Hountalas, D. Kouremenos, Development of a new multi-zone model for the description of physical processes in HCCI engines, Report No. 0148-7191, SAE Technical Paper, 2004.

[69] A.J. Oakley, Experimental investigations on controlled auto-ignition combustion in a four-stroke gasoline engine, Brunel University School of Engineering and Design PhD Theses, 2001.

[70] A. Oakley, H. Zhao, T. Ma, N. Ladommatos, Dilution effects on the controlled auto-ignition (CAI) combustion of hydrocarbon and alcohol fuels, (2001).

[71] A. Oakley, H. Zhao, N. Ladommatos, T. Ma, Experimental studies on controlled auto-ignition (CAI) combustion of gasoline in a 4-stroke engine, Report No. 0148-7191, SAE Technical Paper, 2001.

[72] A. Bhave, M. Kraft, F. Mauss, A. Oakley, H. Zhao, Evaluating the EGR-AFR operating range of a HCCI engine, Report No. 0148-7191, SAE Technical Paper, 2005.

Contact Information

Matteo Pelucchi: matteo.pelucchi@polimi.it, +39 02 02 2399 3243, Department of Chemistry, Materials and Chemical Engineering "G. Natta", Politecnico di Milano, Piazza Leonardo da Vinci 32, 20133, Milan, Italy.

Definitions/Abbreviations

EGR	Exhaust Gas Recirculation
PRF	Primary Reference Fuels
TRF	Toluene Reference Fuels
RON	Research Octane Number
MON	Motor Octane Number
LHV	Lower Heating Value
CN	Cetane Number
SI	Spark Ignition
CI	Compression Ignition
HCCI	Homogeneous Charge Compression Ignition
HRR	Heat Release Rate
PRR	Pressure Release Rate
RCM	Rapid Compression Machine
ST	Shock Tube
BDE	Bond Dissociation Energy
IVC	Intake Valve Closing
EVO	Exhaust Valve Opening
AFR	Air-to-Fuel Ratio
CR	Compression Ratio
CoV	Coefficient of Variation
IMEP	Indicated Mean Effective Pressure
η_{comb}	Combustion Efficiency
TDC	Top Dead Center